BOUNDARY ELEMENTS AND SHEAR BANDS IN INCREMENTAL ELASTICITY

Michele Brun
Davide Bigoni
Dipartimento di Ingegneria Meccanica e Strutturale
Università di Trento
Via Mesiano 77-38050 Povo, Trento, Italia
michele.brun@ing.unitn.it, bigoni@ing.unitn.it

Domenico Capuani
Dipartimento di Ingegneria
Università di Ferrara
Via Saragat 1 - 44100 Ferrara, Italia
cpd@dns.unife.it

Abstract Perturbations in terms of small elastic deformations superimposed upon a given homogeneous strain are analysed within a boundary element framework. This is based on a recently-developed Green's function and boundary integral equations for non-linear incremental elastic deformations. Plane strain deformations are considered of an incompressible hyperelastic solid within the elliptic range. The proposed approach is shown to yield bifurcation loads and modes via a perturbative approach. Numerical treatment of the problem is detailed and applications to multilayers are shown. Relations between shear band formation and global instabilities are given evidence.

1. INTRODUCTION

The response to perturbations of a pre-stressed, non-linear elastic solid is an important issue in a broad spectrum of mechanical problems including the modelling of biological tissues, the analysis of geological formations and the behaviour of seismic insulators and rubber bearings.

With reference to plane strain deformations of incompressible materials, Biot [1] has shown that the incremental elastic response is governed by two incremental moduli, functions of the current stretch. Biot's con-

stitutive framework was assumed in [2] to obtain a Green's function and a boundary integral formulation for incremental deformations superimposed upon a given, homogeneous strain. Both Green's function and integral formulation pave the way for constructing a boundary element technique (BEM) suitable to analyse incremental problems of non-linear elasticity. This is the purpose of the present article, where a general numerical scheme is formulated to handle generic boundary value problems with prescribed nominal tractions or displacement boundary conditions.

It should be mentioned that several attempts have been presented to analyse non-linear problems using boundary element techniques. In these cases, in addition to the usual boundary integrals, a domain integral is introduced, leading to the so-called 'field-boundary element method'. The introduction of this term nullifies a main advantage of BEM and originates from the discrepancy between the nonlinear character of the equations governing the problem and the employed fundamental solution (usually pertinent to linear, isotropic elasticity). Although restricted to perturbations of homogeneously deformed, elastic solids, the proposed boundary element technique retains all the well-known advantages of the small strain formulation, like: discretization limited to the domain boundary; automatic satisfaction of the incompressibility constraint; description of singularities near corner points of the boundary.

The method is shown to be particularly suitable to analyse bifurcation problems even involving surface and localized modes.

2. INCREMENTAL CONSTITUTIVE EQUATIONS

Constitutive equation given by Biot [1] for incompressible materials incrementally deformed in plane strain is adopted. The constitutive framework embraces a broad class of material behaviours including hyper and hypo elasticity, and the loading branch of associated elastoplasticity. In a Lagrangean formulation of field equations, with the current state taken as reference, the constitutive equations for the nominal stress tensor rate $\dot{t}_{ij}$ can be written in the form

$$\dot{t}_{ij} = \mathbb{K}_{ijkl} v_{l,k} + \dot{p}\delta_{ij} = \tilde{\mathbb{K}}_{ijkl} v_{l,k} + \dot{\pi}\delta_{ij}, \quad v_{i,i} = 0, \tag{1.1}$$

where v_i is the velocity, δ_{ij} is the Kronecker delta and

$$\dot{p} = \frac{\dot{\sigma}_1 + \dot{\sigma}_2}{2}, \qquad \dot{\pi} = \frac{\dot{t}_{11} + \dot{t}_{22}}{2} = \dot{p} - \frac{\sigma_1 - \sigma_2}{2} v_{1,1}, \tag{1.2}$$

are the in plane hydrostatic stress rates (positive in tension), related to the principal components σ_1, σ_2 of the Cauchy stress and to the

nominal stress. The tensor $\mathbb{K}_{ijkl}$ represents the instantaneous stiffness, characterised by the major symmetry $\mathbb{K}_{ijkl} = \mathbb{K}_{klij}$ and having the form [3]

$$\begin{aligned}
&\mathbb{K}_{1111} = \mu_* - \frac{\sigma}{2} - p, \quad \mathbb{K}_{1122} = -\mu_*, && \mathbb{K}_{1112} = \mathbb{K}_{1121} = 0,\\
&\mathbb{K}_{2211} = -\mu_*, && \mathbb{K}_{2222} = \mu_* + \frac{\sigma}{2} - p, && \mathbb{K}_{2212} = \mathbb{K}_{2221} = 0,\\
&\mathbb{K}_{1212} = \mu + \frac{\sigma}{2}, && \mathbb{K}_{1221} = \mathbb{K}_{2112} = \mu - p, && \mathbb{K}_{2121} = \mu - \frac{\sigma}{2},
\end{aligned} \tag{1.3}$$

where

$$\sigma = \sigma_1 - \sigma_2, \qquad p = \frac{\sigma_1 + \sigma_2}{2}, \tag{1.4}$$

and μ, μ_* are two incremental moduli corresponding respectively to shearing parallel to, and at 45° to, the Eulerian principal axes.

The formulation is restricted to the elliptic range (E), corresponding to negative or complex coefficients γ_1 and γ_2:

$$\left.\begin{matrix}\gamma_1\\ \gamma_2\end{matrix}\right\} = \frac{1 - 2\dfrac{\mu_*}{\mu} \pm \sqrt{\Delta}}{1+k}, \quad \Delta = k^2 - 4\frac{\mu_*}{\mu} + 4\left(\frac{\mu_*}{\mu}\right)^2, \tag{1.5}$$

where $k = \sigma/(2\mu)$ is a parameter characterising the pre-stress. The elliptic range may be further sub-divided into elliptic-imaginary (EI: $\Delta > 0$, so that γ_1 and γ_2 are both negative) and elliptic-complex (EC: $\Delta < 0$, so that γ_1 and γ_2 are a conjugate pair) regimes.

Discontinuous strain rates corresponding to shear bands are possible at the boundary of the elliptic range. Elliptic imaginary/parabolic (EI/P) boundary is attained when $k = 1$ ($\gamma_1 = 0$) whereas elliptic complex/hyperbolic (EC/H) boundary is attained when $\Delta = 0$ ($\gamma_1 = \gamma_2$).

3. THE FUNDAMENTAL SOLUTION

In the framework described by the constitutive eqns. (1.1), the Green's function set $\{v_i^g; \dot{\pi}^g\}$ for an infinite and uniformly deformed medium can be written in the form [2]:

$$\begin{aligned}
v_i^g \;=\; & \frac{1}{2\pi^2\mu(1+k)}\left\{\frac{\pi\,\delta_{ig}\,\log r}{[(2-i)\,\gamma_2 + 1 - i]\,\sqrt{-\gamma_1} + [(2-i)\,\gamma_1 + 1 - i]\,\sqrt{-\gamma_2}}\right.\\
& \left. - \int_0^{\frac{\pi}{2}} [K_i^g(\alpha+\theta) + (3-2i)\,(3-2g)\,K_i^g(\alpha-\theta)]\log(\cos\alpha)\,d\alpha\right\},
\end{aligned} \tag{1.6}$$

$$\dot{\pi}^g = -\frac{1}{2\pi r}\left\{\cos\Big[\theta-(g-1)\frac{\pi}{2}\Big]+\frac{1}{\pi(1+k)}\int_0^\pi \frac{\tilde{K}_g\,(\alpha+\theta)}{\cos\alpha}d\alpha\right\}, \tag{1.7}$$

where r and θ are the polar coordinates singling out the generic point with respect to the position $\mathbf{y}$ of the concentrated force, indices i and g range between 1 and 2 and

$$K_i^g(\alpha)=\frac{\sin\left[\alpha+(i-1)\frac{\pi}{2}\right]\sin\left[\alpha+(g-1)\frac{\pi}{2}\right]}{\Lambda\,(\alpha)}, \tag{1.8}$$

$$\Lambda(\alpha)=\sin^4\alpha(\cot^2\alpha-\gamma_1)(\cot^2\alpha-\gamma_2)>0, \tag{1.9}$$

$$\tilde{K}_g(\alpha)=K_g^g(\alpha)\,\cos\Big[\alpha+(g-1)\frac{\pi}{2}\Big]\,\Gamma(\alpha),\quad (g \text{ not summed}) \tag{1.10}$$

$$\Gamma(\alpha)=2\left(\frac{\mu_*}{\mu}-1\right)\left(2\cos^2\alpha-1\right)-k. \tag{1.11}$$

From the Green's velocity v_i^g and pressure rate $\dot{\pi}^g$, the in-plane hydrostatic stress rate $\dot{p}^g$ and the associated incremental nominal stress $\dot{t}_{ij}^g$ can be obtained by using constitutive equations (1.1).

4. BOUNDARY ELEMENT FORMULATION

We refer to mixed boundary value problems in which velocities and incremental nominal tractions $\dot{\tau}$ are prescribed functions

$$v_i=\bar{v}_i,\ \text{on}\ \partial B_v,\qquad \dot{t}_{ij}n_i=\dot{\bar{\tau}}_j\ \text{on}\ \partial B_\tau,\quad \partial B=\partial B_v\cup\partial B\tau, \tag{1.12}$$

defined on separate portions ∂B_v and ∂B_τ of the boundary ∂B of a solid B, currently in a state of homogeneous, finite deformation.

In this context, an integral representation exists relating the velocity at interior points of the body to the boundary values of nominal traction rates and velocities [2]:

$$v_g(\mathbf{y})=\int_{\partial B}\Big[\dot{t}_{ij}(\mathbf{x})\,n_i(\mathbf{x})\,v_j^g(\mathbf{x},\mathbf{y})-\dot{t}_{ij}^g(\mathbf{x},\mathbf{y})\,n_i(\mathbf{x})\,v_j(\mathbf{x})\Big]\,dl_x. \tag{1.13}$$

If the point $\mathbf{y}$ is at the boundary, eqn.(1.13) becomes [2]

$$C_j^g v_j(\mathbf{y}) = \int_{\partial B}\dot{\tau}_j(\mathbf{x})\,v_j^g(\mathbf{x},\mathbf{y})\,dl_x-\fint_{\partial B}\dot{\tau}_j^g(\mathbf{x},\mathbf{y})\,v_j(\mathbf{x})\,dl_x, \tag{1.14}$$

where

$$C_i^g=\lim_{\varepsilon\to 0}\int_{\partial C_\varepsilon}\dot{\tau}_i^g(\mathbf{x},\mathbf{y})\,dl_x, \tag{1.15}$$

is the so-called **C**-matrix, depending on the material parameters, state of pre-stress and the geometry of the boundary (in the case of a smooth boundary, $C_i^g = \frac{1}{2}\delta_{gi}$). Note that symbol ∂C_ε introduced in (1.15) denotes the intersection between a circle of radius ε centred at $\mathbf{y}$ and the domain B.

The boundary equation (1.14) is the starting point to derive the *collocation boundary element method*. To this purpose, the boundary ∂B is divided into m elements Γ^e $(e = 1, \cdots, m)$, with subsets m_u and m_τ belonging respectively to ∂B_u and ∂B_τ (clearly $m = m_u + m_\tau$).

Inside each boundary element Γ^e, the following discretization for velocities and nominal tractions is introduced

$$\begin{aligned} v_i(\mathbf{x}) &= \varphi_\alpha(\mathbf{x})\, \bar{v}_{i\alpha}, \\ \dot{\tau}_i(\mathbf{x}) &= \varphi_\alpha(\mathbf{x})\, \dot{\bar{\tau}}_{i\alpha}, \qquad\qquad \alpha = 0, \cdots, \Theta, \end{aligned} \tag{1.16}$$

where $\bar{v}_{i\alpha}$, $\dot{\bar{\tau}}_{i\alpha}$ are the nodal values of velocities and nominal traction rates, respectively, and φ_α are the relevant shape functions, selected as polynomials of degree Θ.

The discretized form of eqn. (1.14), collocating the point $\mathbf{y}$ at $\mathbf{y}^{(\bar{e},\bar{\alpha})}$, corresponding to the node $\bar{\alpha}$ of the element $\bar{e}$ is:

$$C_i^g \bar{v}_{i\bar{\alpha}}^{\bar{e}} + \sum_{e=1}^{m} \left(\bar{v}_{i\alpha}^e \int_{\Gamma^e} \varphi_\alpha(\mathbf{x})\, \dot{\tau}_i^g(\mathbf{x},\mathbf{y}) dl_x - \dot{\bar{\tau}}_{i\beta}^e \int_{\Gamma^e} \psi_\beta(\mathbf{x})\, v_i^g(\mathbf{x},\mathbf{y}) dl_x \right) = 0, \tag{1.17}$$

where indices α and i are summed and range between $0 - \Theta$ and $1 - 2$, respectively.

Collocating eqn. (1.17) at each node along the two directions x_1 and x_2 yields an algebraic system that can be written in a form

$$\mathbf{H}\hat{\mathbf{v}} = \mathbf{G}\dot{\hat{\tau}}, \tag{1.18}$$

where $\hat{\mathbf{v}}$ and $\dot{\hat{\tau}}$ are the vectorial expressions for $\bar{v}_{i\alpha}^e$ and $\dot{\bar{\tau}}_{i\beta}^e$, defined as:

$$\hat{v}_{2\Theta(e-1)+2\alpha+i} = \bar{v}_{i\alpha}^e, \qquad\qquad \hat{\tau}_{2\Theta(e-1)+2\alpha+i} = \dot{\bar{\tau}}_{i\alpha}^e, \tag{1.19}$$

where Θ is not a free index, but the fixed number specifying the degree of the interpolating functions.

Solution of system (1.18), after re-arrangement of data and unknowns, gives the nodal velocities $\bar{v}_{i\alpha}$ on ∂B_τ, and the nominal traction rates $\dot{\bar{\tau}}_{i\beta}$ on ∂B_v.

We limit the presentation to discretization of the boundary into linear elements and linear shape functions, so that the singular integrals in eqn. (1.17) relative to elements adjacent to the collocation node e can

be evaluated analytically. In particular, the strongly singular integral on the left hand side of eqn. (1.17), after change of variable, takes the form

$$I_{strong}^{(ig,e)} = \int_0^{l_{e-1}} \left(1 - \frac{\eta}{l_{e-1}}\right) \dot{\tau}_i^g(\eta, \theta_1)\, d\eta + \int_0^{l_e} \left(1 - \frac{\eta}{l_e}\right) \dot{\tau}_i^g(\eta, \theta_2)\, d\eta. \tag{1.20}$$

As far as the two elements $e-1$ and e are concerned, the incremental Green's tractions can be computed as:

$$\tau_i^g(r) = (-1)^e \frac{\chi_{ig}(k, \frac{\mu_*}{\mu})}{r}, \tag{1.21}$$

which are independent of θ. Introducing eqn. (1.21) into eqn. (1.20), we obtain

$$I_{strong}^{(ig,e)} = (-1)^e\, \chi_{ig} \log\left(\frac{l_e}{l_{e-1}}\right). \tag{1.22}$$

Analogously, the weakly singular integral on the right hand side of eqn. (1.17) is equal to

$$I_{weak}^{(ig,e)} = \int_0^{l_{e-1}} \left(1 - \frac{\eta}{l_{e-1}}\right) v_i^g(\eta, \theta_1)\, d\eta + \int_0^{l_e} \left(1 - \frac{\eta}{l_e}\right) v_i^g(\eta, \theta_2)\, d\eta. \tag{1.23}$$

Taking in account the expression of v_i^g given in eqn.(1.6) the integral (1.23) can be analytically evaluated and the resulting four components are listed in Table (1).

Table 1 Analytic expressions for the weakly singular integrals (1.23)

i	g	*Integral* $I_{weak}^{(ig,e)}$
1	1	$\frac{l_{e-1}}{2}\left[\frac{2\log(l_{e-1})-3}{D_{11}} + v_1^1(1,\theta_1)\right] + \frac{l_e}{2}\left[\frac{2\log(l_e)-3}{D_{11}} + v_1^1(1,\theta_2)\right]$
1	2	$\frac{l_{e-1}}{2}\, v_1^2(\theta_1) + \frac{l_e}{2}\, v_1^2(\theta_2)$
2	1	$\frac{l_{e-1}}{2}\, v_2^1(\theta_1) + \frac{l_e}{2}\, v_2^1(\theta_2)$
2	2	$\frac{l_{e-1}}{2}\left[-\frac{2\log(l_{e-1})-3}{D_{22}} + v_2^2(1,\theta_1)\right] + \frac{l_e}{2}\left[-\frac{2\log(l_e)-3}{D_{22}} + v_2^2(1,\theta_2)\right]$

$D_{11} = 4\mu\pi(1+k)(\gamma_2\sqrt{-\gamma_1} + \gamma_1\sqrt{-\gamma_2})$, $D_{22} = 4\mu\pi(1+k)(\sqrt{-\gamma_1} + \sqrt{-\gamma_2})$

5. NUMERICAL EXAMPLES

As a first example, the response of a multilayered elastic block to an incremental, skew-symmetric loading $\dot{\tau}$, (see the detail in Fig. 1) is investigated. The block is formed by three layers perfectly bonded to each other. Material (1) constituting the external layers is supposed to be different from material (2) of the inner layer. All layers are supposed to undergo the same homogeneous, plane strain deformation with the principal directions of deformation aligned normal and parallel to the layers. Therefore, a uniaxial state of traction or compression prevails in the laminate, with different values for materials 1 and 2. Starting from this pre-stressed state, the incremental load $\dot{\tau}$ is applied. The loaded zone has been chosen to be equal to 2/15 b (b is the half-length of the edges) and a regular boundary mesh for each layer has been adopted.

Three ratios of incremental shear moduli $(\mu_*/\mu)_1$, $(\mu_*/\mu)_2$ and μ_1/μ_2 have been considered for the two materials (Tab. 2) and the relevant results are shown in Fig. 1, where the velocity [normalized through multiplication by $\mu_1/(b\dot{\tau})$] is plotted versus the pre-stress k. It can be seen

Table 2 Bifurcation stress k for a three-layered elastic structure

Example	*Shear moduli ratios*			*Bifurcation stress k*	
	$(\mu_*/\mu)_1$	$(\mu_*/\mu)_2$	μ_1/μ_2	*Analytical*	*Numerical*
1	1.0	0.5	0.5	0.4722	0.4852 ÷ 0.4859
2	0.5	1.0	2.0	0.3714	0.3789 ÷ 0.3797
3	2/3	1.0	1.5	0.4386	0.4469 ÷ 0.4477

that traction increases stiffness whereas compression induces stiffness degradation, which becomes dramatic when critical values of k are approached. Tab. 2 compares numerical estimates of the bifurcation values of k with those evaluated analytically by Bigoni and Gei [4], though for slightly different boundary conditions. It is worth noting that the value of k is independent of the material, but depends only on the maximum in-plane stretch.

A second example concerns the so-called 'van Hove condition', where the solid is subjected to prescribed displacements over the entire boundary and the current deformation (and stress) is homogeneous [5, 6]. In these conditions, starting from an unloaded configuration, shear bands occur as the first possible bifurcation. We analyse this situation for the square elastic block shown in Fig. 2, characterised by $\mu_*/\mu = 0.25$ (corresponding to the elliptic complex regime) and homogeneously de-

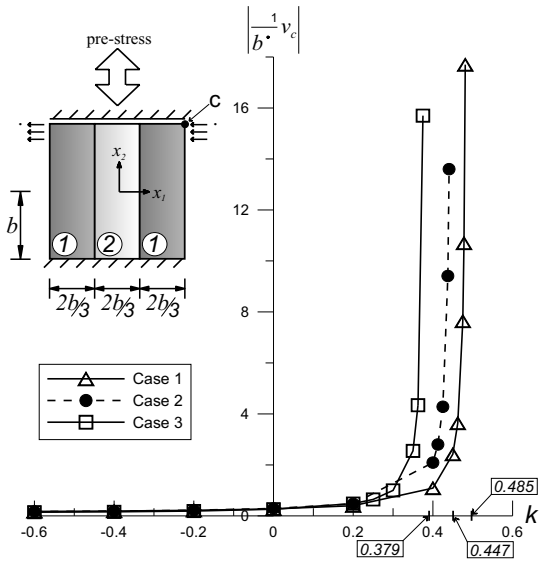

Figure 1 Non-dimensionalized velocity of the corner point c versus pre-stress k.

formed in a state of uniaxial tension and compression. All displacements are prescribed on the boundary, so that the solution is known unless an arbitrary value of homogeneous pressure. A perturbation is given by prescribing the triangular distribution of velocity sketched in Fig. 2. The level sets of the modulus of the velocity are reported in Fig. 3 and

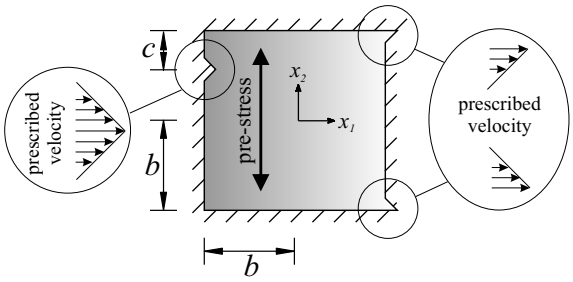

Figure 2 Loading geometry in van Hove conditions.

4, for three different values of pre-stress $k = \{-0.859, 0, 0.859\}$. The values ± 0.859 are close to the boundary of loss of ellipticity (± 0.866),

where shear bands become possible, inclined at an angle $\eta = 27.367°$, with respect to the direction of tensile stress.

The fact that strain localization can be observed within the elliptic range — employing a perturbation approach — agrees with previous findings [2, 7]. This aproach may provide an explanation of the fact that shear banding is a preferred instability when compared to other diffuse bifurcations, possible at loss of ellipticity under van Hove conditions [8].

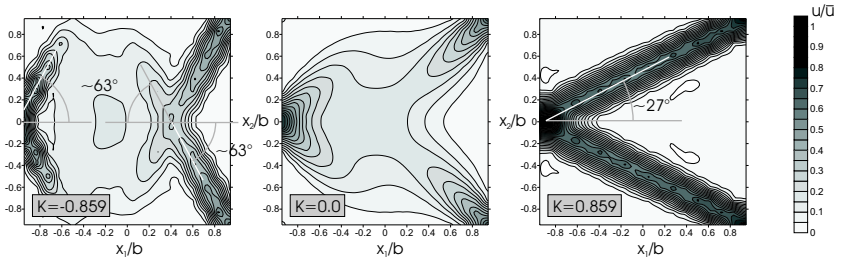

Figure 3 Level sets of modulus of velocity at different values of pre-stress k. Loading geometry is sketched in Fig. 2, with $c/b = 1/2$. Note the shear bands emerging at $k = \pm 0.859$.

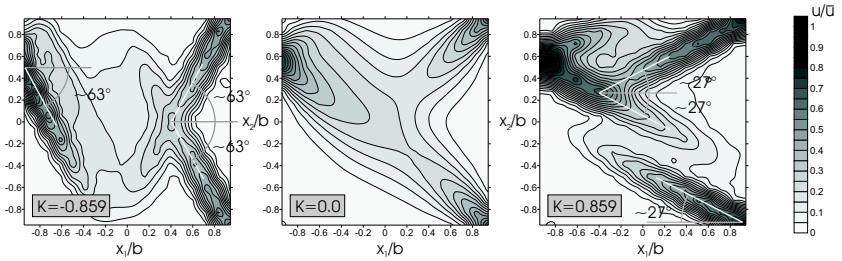

Figure 4 Level sets of modulus of velocity at different values of pre-stress k. Loading geometry is sketched in Fig. 2, with $c/b = 4/9$. Note the shear bands emerging at $k = \pm 0.859$.

The van Hove setting is very peculiar and provides the maximum possible 'confinement' to a material sample. A relaxation of this severe configuration was proposed by Ryzhak [9] and will be called 'weak van Hove' conditions in the following. In particular, the material must be homogeneous and orthotropic, with orthotropy axes parallel and orthogonal to the given loading direction. Two parallel edges of the material element must be in smooth (bilateral) contact with a rigid constraint. The current configuration, sketched in Fig. 5, is perturbed with two assigned, triangular velocity distributions. For weak van Hove conditions, level sets of the modulus of the velocity are plotted in Figs. 6 and

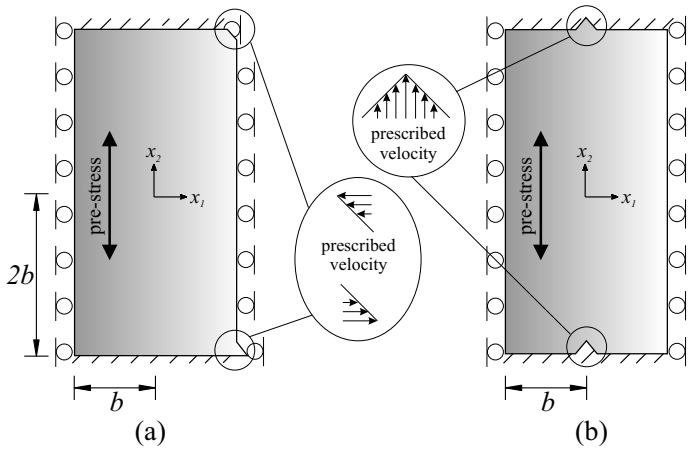

Figure 5 Loading geometries in weak van Hove conditions.

7, for different values of pre-stress $k = \{0, 0.7, 0.857\}$, corresponding to compression parallel to x_2.

It can be seen that shear banding is not evident until $k = 0.7$ but it appears clearly for $k = 0.857$, which is close to the boundary of ellipticity. 'Reflection' of shear bands at the boundary emerges as a peculiar deformation pattern. Similar deformation mechanisms have been also observed in different contexts (porous plastic materials [10]; dynamics of visco-plastic solids [11, 12]), and may explain pattern formation in biological system or geological structures. The localization of deformation may also suggest possible technological applications. For instance, the highly strained regions could be employed to transmit signals so that the pre-stress could become a parameter controlling special types of delay lines.

Acknowledgments

Financial support of the University of Trento (D.B. and M.B.) and of the University of Ferrara (D.C.) is gratefully acknowledged.

References

[1] Biot, M A (1965) *Mechanics of incremental deformations*. J. Wiley and Sons, New York.

[2] Bigoni, D and Capuani, D (2002) *J. Mech. Phys. Solids* **50**, 471-500.

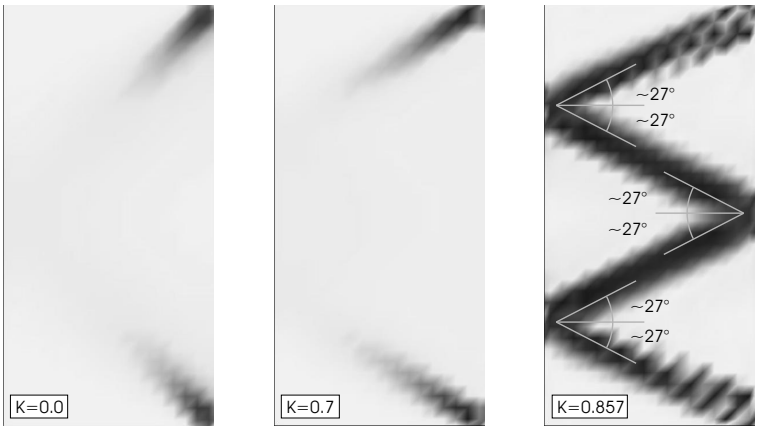

Figure 6 Level sets of modulus of velocity at different values of pre-stress k. Loading geometry is sketched in Fig. 5(a). Note the shear bands emerging at $k = 0.857$.

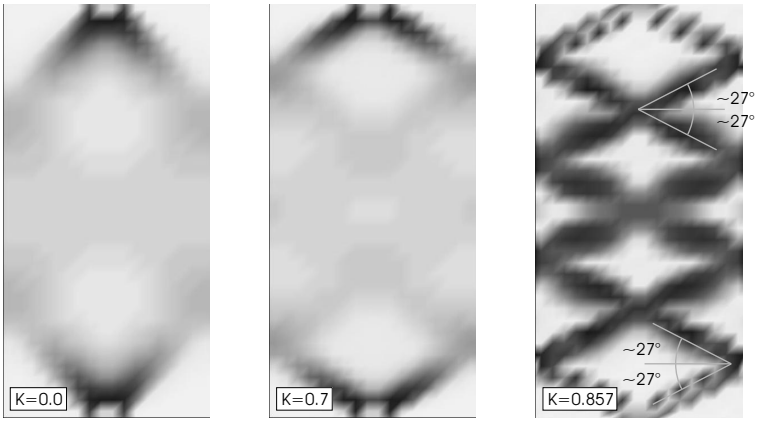

Figure 7 Level sets of modulus of velocity at different values of pre-stress k. Loading geometry is sketched in Fig. 5(b). Note the shear bands emerging at $k = 0.857$.

[3] Hill, R and Hutchinson, J W (1975) *J. Mech. Phys. Solids* **23**, 239-264.

[4] Bigoni, D and Gei, M (1999) On bifurcation of a layered, orthotropic, elastic medium. XXVIII AIAS National Congress, Vicenza, Italy, 8-11 September 1999.

[5] van Hove, L (1947) *Proc. Sect. Sci. K. Akad. van Wetenschappen*, Amsterdam **50**, 18-23.

[6] Bigoni, D (2000) Bifurcation and instability of non-associative elastic-plastic solids. *CISM Lecture Notes No. 414 "Material Instabilities in Elastic and Plastic Solids", H. Petryk*, Ed. Springer-Verlag, Wien-New York.

[7] Radi, E, Bigoni, D and Capuani, D (2002) *Int. J. Solids Structures* **39**, 3971-3996.

[8] Ryzhak, E I (1999) *Int. J. Solids Structures* **36**, pp. 4669-4691.

[9] Ryzhak, E I (1993) *J. Mech. Phys. Solids* **41**, 1345-1356.

[10] Tvergaard, V (1982) *J. Mech. Phys. Solids* **30**, 399-425.

[11] Deb, A, Prevost, J H and Loret, B (1996) *Comput. Meth. Appl. Mech. Engrg.* **137**, 285-306.

[12] Deb, A, Loret, B and Prevost, J H (1996) *Comput. Meth. Appl. Mech. Engrg.* **137**, 307-330.